13

Magnetic Exchange Force Microscopy

Alexander Schwarz, Uwe Kaiser, Rene Schmidt, and Roland Wiesendanger

Abstract. Magnetic exchange force microscopy is a novel noncontact atomic-force microscopy based technique to image the arrangement of magnetic moments at surfaces with atomic resolution using sharp magnetic tips. Recent results obtained with iron coated silicon tips on two magnetically different antiferromagnetic surfaces are reviewed: NiO(001), an insulator, where the localized spin-carrying d-electrons are localized and interact via superexchange and Fe/W(001), a metal with delocalized itinerant spin-carrying d-electrons. The experimental findings are discussed with respect to the tip configuration, the role of an applied magnetic field, the magnitude of the magnetic signal as well as the interplay between chemical and magnetic forces.

13.1 Introduction

New developments in the field of magnetic imaging are fueled by demands of novel magnetic data storage and sensor devices as well as a fundamental interest in magnetic phenomena. This tendency is generally evident in the history of scanning probe microscopy. Thus, shortly after the invention of scanning tunneling microscopy (STM) in 1982 [1] and atomic force microscopy (AFM) in 1986 [2], their high resolution capabilities were utilized for magnetic sensitive imaging by implementing magnetic tips. One year after the invention of AFM, magnetic force microscopy (MFM) was established [3], and is now widely used [4]. It senses the long-range dipolar magnetostatic force between a ferromagnetic tip and a ferromagnetic sample. Imaging is performed in the constant height mode. Typical tip–sample distances are larger than 10 nm to separate the magnetic signal from topographical features. This relatively large scan height as well as the spreading of the stray field emanating from the tip limits the resolution to about 10 nm [5].

A much higher resolution is possible with spin-polarized scanning tunneling microscopy (SP-STM), which was invented in 1990 [6], and is nowadays routinely used to image metallic magnetic surfaces with atomic resolution [7]. A method based on force detection, which therefore can also be applied to

S. Morita et al. (eds.), *Noncontact Atomic Force Microscopy*,
NanoScience and Technology,
DOI: 10.1007/978-3-642-01495-6_13, © Springer-Verlag Berlin Heidelberg 2009

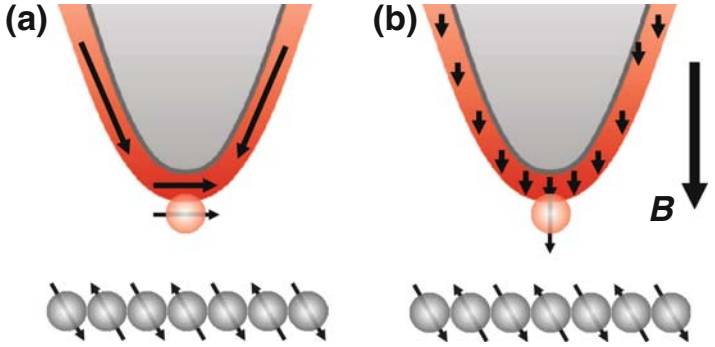

Fig. 13.1. Concept of MExFM on antiferromagnetic surfaces. The magnetic exchange force between tip and sample can be unambiguously discriminated from the chemical force, if atoms, which are chemically and structurally identical, possess oppositely oriented magnetic moments. (**a**) In-plane sensitive tip apex. If shape anisotropy dominates, ferromagnetic thin film tips are in this configuration. (**b**) Out-of-plane sensitive tip apex. Such a configuration can be realized by applying a sufficiently large external flux density B perpendicular to the surface

insulating surfaces, i.e., magnetic exchange force microscopy (MExFM), was proposed as early as 1991 [8]. However, it was not realized until 2007 [9], when atomic-scale imaging with magnetic sensitivity on the antiferromagnetic NiO(001) was reported for the first time.[1] The general set-up resembles that of an NC-AFM experiment [11], except that for MExFM the atomically sharp tip, which is approached close to the surface, has to be magnetically sensitive as well (cf. Fig. 13.1). At sufficiently small distances the spin-carrying electronic states of the foremost tip atom and the surface atom directly underneath overlap resulting in a significant magnetic exchange interaction. In the simplest approximation, the magnetic exchange interaction between magnetic moments of the foremost tip atom and the surface atom directly underneath, can be described by a Heisenberg model, i.e., $E_{\mathrm{ex}} = -J\boldsymbol{S}_{\mathbf{t}}\boldsymbol{S}_{\mathbf{s}}$, where J is the exchange coupling constant between tip and sample spins $\boldsymbol{S}_{\mathbf{t}}$ and $\boldsymbol{S}_{\mathbf{s}}$, respectively. Magnitude and sign of the magnetic exchange energy E_{ex} depends on the relative orientation between $\boldsymbol{S}_{\mathbf{t}}$ and $\boldsymbol{S}_{\mathbf{s}}$ as well as on the the sign of J, i.e., positive for ferromagnetic coupling and negative for antiferromagnetic coupling. Hence, on antiferromagnetically ordered surfaces (see sketch in Fig. 13.1) an alternating contrast that varies on the atomic scale is expected.

[1] Previous reports of a magnetic contrast on NiO(001) [10] were ambiguous and probably even wrong, because (1) no magnetic signal could be seen in the raw data, (2) a Fourier transform to prove that the antiferromagnetic periodicity was really detected was never presented, and (3) the claimed magnetic contrast in an unit cell averaged image was seen between neighboring rows of oxygen atoms and not between neighboring rows of nickel atoms.

In the following sections, we review MExFM experiments performed at low temperatures in ultra-high vacuum with our home-built microscope (*Hamburg design*) [12] using ferromagnetic iron tips on two antiferromagnetic sample systems: NiO(001) [9,13] and the Fe monolayer on W(001) [14–16]. On these two samples chemical and magnetic interactions, which are both electron mediated and short-ranged, can be unambiguously distinguished from each other, because the antiferromagnetically ordered magnetic moments are located at chemically and structurally equivalent atomic sites. Moreover, an external magnetic field can be applied to align the magnetic moments of the ferromagnetic tip into a favorable direction without altering the antiferromagnetic structure of the sample. We will discuss mainly the experimental aspects of MExFM, e.g., contrast pattern, magnitude of chemical and magnetic signal, tip properties, etc. First-principles calculations based on density functional theory, which go far beyond the simple Heisenberg model mentioned earlier, are presented in Chap. 14 of this book [16].

13.2 Tip Preparation

The precise atomic configuration at the tip-apex region plays an important role for atomic resolution imaging, e.g., it will influence the magnitude of the corrugation amplitude and whether a certain chemical species appears as protrusion or depression. The situation is obviously even more complex, if one has to consider magnetic exchange interactions as well. Unfortunately, not much is usually known about the actual configuration of atoms at the tip apex. In fact, the sample is often much better characterized than the tip in most scanning probe experiments. Nevertheless, some general assumptions regarding the configuration at the tip-apex can be inferred.

The direction of the magnetic moment of the foremost tip atom depends on magnetic exchange energy, magneto-crystalline anisotropy energy, shape anisotropy energy and Zeeman energy. In bulk iron the easy axis of magnetic polarization is along ⟨001⟩-directions due to the magneto-crystalline anisotropy energy. If silicon tips are coated with a thin iron film, e.g., about 10–20 nm, shape anisotropy favors a magnetic polarization parallel to the surface at the tip apex (cf. Fig. 13.1a), but with no a priori preferred orientation within this plane [5]. A magnetic polarization perpendicular to the surface can be induced by an external magnetic flux density oriented parallel to the tip axis (cf. Fig. 13.1b). However, some of our experimental results indicate that even if the applied external magnetic flux density (e.g., 5 T) is larger than the saturation magnetic polarization of iron (2.187 T), the foremost tip atom is not necessarily aligned accordingly [13]. Probably, local magnetic anisotropy energies dominate at the tip-apex, where atoms are certainly not in a bulk-like configuration.

During atomic resolution imaging in NC-AFM experiments spontaneous tip changes are frequently observed due to the strong interaction between tip

and sample at small distances. Particularly, one tip configuration might be suitable for atomic resolution, but another one might not be, e.g., because the tip-apex does not end in a single atom. In MExFM experiments tip changes can additionally switch between magnetically sensitive and magnetically insensitive tip configurations. For example, after a collision between tip and sample either a non-magnetic adsorbate could be picked up or all magnetic atoms at the tip apex could be lost. However, even if the tip apex is covered with magnetic material and atomically sharp, it might still be impossible to resolve the magnetic structure. For example, the direction of the magnetic moment of the tip is not stable, e.g., it rotates randomly on a time scale much faster than the data acquisition time or it aligns itself always parallel (or antiparallel) to the surface magnetic moments. Another possibility is a too low signal-to-noise ratio. For example, the angle between magnetic moments of foremost tip-apex atom and surface atoms could be close to 90°, the magnetic moments could be too small or the tip–sample distance could be too large.

Although spontaneous unwanted tip changes are bothersome in general, intented collisions between tip and sample can be utilized to provoke tip changes. This is routinely done in NC-AFM experiments to achieve atomic resolution with an initially blunt tip-apex. Similarly, it is also possible to obtain a magnetically sensitive tip configuration in this manner. Whatever the real configuration at the tip-apex is, if atomic resolution is obtained in the noncontact regime, one can at least infer that the tip-apex is atomically sharp.

The easiest way to unambiguously distinguish between magnetic insensitive and magnetic sensitive tip configurations is to perform measurements on surfaces, where structurally and chemically identical atoms are antiferromagnetically ordered. On ferromagnetic surfaces the situation is more delicate. One way is to look for domain walls, where the direction of the magnetic moments change continuously. Another possibility would be to either reverse the magnetic polarization of the sample or the tip (but not both simultaneously), which would result in a contrast reversal between two MExFM images recorded on precisely the same area. However, to assure registry on the atomic level, a marker defect, e.g., a vacancy or an adsorbate, has to be present in the imaged area.

13.3 NiO(001)

Nickel oxide (cf. Fig. 13.2a), crystallizes in the rock salt structure ($a = 417\,\mathrm{pm}$) and exhibits a nearly perfectly bulk terminated (001) surface [17] with a (1×1) chemical surface unit cell. Below its Néel temperature of 525 K, it is a collinear antiferromagnet. Magnetic moments point in $\langle 211\rangle$ directions and are coupled ferromagnetically in $\{111\}$ planes, which are stacked in an antiferromagnetic order due to the superexchange of the localized nickel d-electrons via the bridging oxygen atoms. Since the magnetic order is bulk terminated as well [18], the (001) surface shows a row-wise antiferromagnetic order with a (2×1)

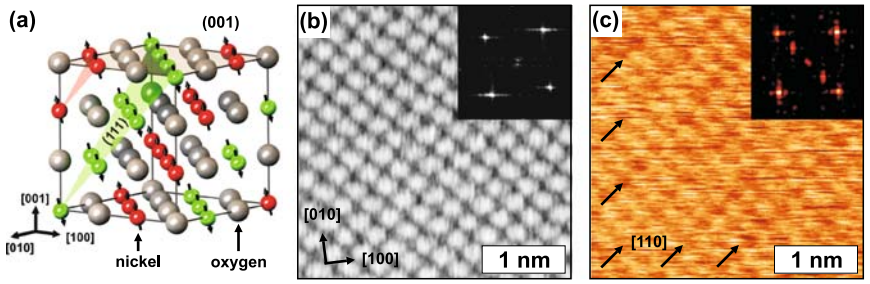

Fig. 13.2. (**a**) Rock salt structure of nickel oxide. The (001) surface exhibits a checkerboard pattern of Ni- and O-atoms with an antiferromagnetic ordering between neighboring rows of Ni-atoms along ⟨110⟩-directions. (**b**) NC-AFM image on NiO(001). Oxygen atoms are imaged as protrusions and nickel atoms as depressions. The fourier transform (*inset*) shows four peaks, representing the chemical surface unit cell. (**c**) MExFM image of NiO(001). Neighboring rows of depressions, i.e., nickel atoms, exhibit slightly different contrast levels, which shows up as an additional pair of peaks in the fourier transform (inset). Parameters: (**b**) $f_0 = 165\,\mathrm{kHz}$, $c_z = 36.0\,\mathrm{N/m}$, $A_0 = \pm 15\,\mathrm{nm}$, $\Delta f = -11.0\,\mathrm{Hz}$ and (**c**) $B = 5\,\mathrm{T}$, $f_0 = 159\,\mathrm{kHz}$, $c_z = 36.0\,\mathrm{N/m}$, $A_0 = \pm 6.7\,\mathrm{nm}$, $\Delta f = -23.4\,\mathrm{Hz}$

magnetic surface unit cell. Clean NiO(001) samples with some 10 nm wide and clean terraces separated by monatomic steps (cf. Fig. 13.2a), are prepared by in situ cleavage of single crystals and subsequent heating to remove surface charges.

Figure 13.2b displays a typical NC-AFM image recorded with a non-magnetic tip [19–21]. The arrangement of maxima and minima as well as the four peaks in the Fourier transform, cf. inset, clearly reflects the (1×1) chemical surface unit cell. It is most likely that maxima correspond to the position of the oxygen atoms, where the total valence charge density is largest [22], and hence the electron mediated chemical interaction responsible for the atomic scale contrast is expected to be largest as well [23]. The chemical corrugation amplitude of about 20 pm is well above the noise level of our instrument.

On the other hand, Fig. 13.2c shows an MExFM image recorded with an iron coated tip. First, the overall corrugation amplitude of about 5 pm is much lower compared to Fig. 13.2a. Second, the raw data exhibit a small contrast between neighboring rows of minima, which shows up as additional pair of peaks in the Fourier transform, cf. inset, and corresponds to the larger (2×1) magnetic surface unit cell. Even though the signal-to-noise ratio in the raw image data is low, these two peaks in the Fourier transform unambiguously prove the detection of the antiferromagnetic structure. To determine the corrugation amplitude quantitatively, we performed a unit cell averaging procedure.[2] For a better visualization of the periodicity of the antiferromag-

[2] All unit cells in the raw data of a periodic image can be averaged to obtain a single averaged unit cell of much better signal-to-noise ratio. This procedure to enhence the image quality is well established in the field of electron microscopy.

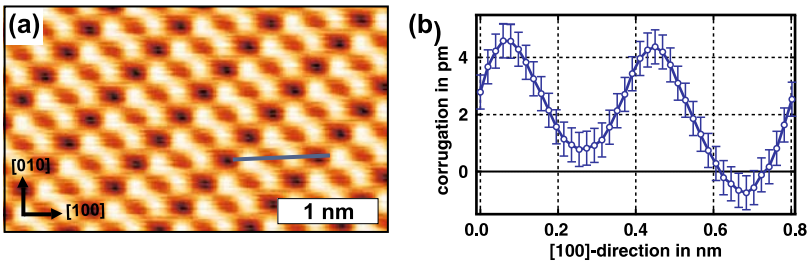

Fig. 13.3. (**a**) Unit cell averaged image of the raw data displayed in Fig. 13.2c. (**b**) Line section along the [001] direction of NiO(001). The magnetic contrast between neighboring rows of Ni-atoms (minima) is about 1.5 pm. No contrast is visible between neighboring rows of O-atoms (maxima)

netic structure the image in Fig. 13.3a is tiled from the averaged unit cell and clearly shows the row-wise modulation due to the magnetic exchange interaction between the ferromagnetic iron tip and the antiferromagnetic NiO(001) surface. From the line section along the [100]-direction, cf. Fig. 13.3b, a chemical corrugation amplitude of $z_{\mathrm{chem}} = \frac{1}{2}|(\mathrm{Ni}\uparrow - \mathrm{O}) - (\mathrm{Ni}\downarrow - \mathrm{O})| = 4.5\,\mathrm{pm}$ and a magnetic corrugation amplitude of $z_{\mathrm{mag}} = |\mathrm{Ni}\uparrow - \mathrm{Ni}\downarrow| = 1.5\,\mathrm{pm}$ can be measured.

Interestingly, we found that on approaching the surface by adjusting larger negative frequency shifts we first see only a chemical contrast but at smaller distances the magnetic contrast appears as additional modulation on top of the nickel atoms [9]. The origin of this distance dependent contrast are the localized spin-carrying *d*-electrons, which do not reach as far as the *s*- and *p*-electrons into the vacuum region. Peculiarly, the chemical contrast in the MExFM experiment, cf. Fig. 13.2b, is much lower than in the normal NC-AFM experiments, cf. Fig. 13.2a. Since we always observe a rather small chemical corrugation amplitude in our MExFM experiment on NiO(001), tips with a small chemical interaction might be required to approach close enough to the surface to probe the localized *d*-electrons. A large chemical interaction might otherwise lead to a tip instability before any magnetic signal is detectable.

The contrast pattern in Fig. 13.2c is the regular MExFM contrast on NiO(001), which is in qualitative agreement with theoretical predictions of a significant magnetic exchange force between the magnetic moments of a single atom iron tip and the nickel atoms in NiO(001) [24]. However, in Fig. 13.4a a modulation of the corrugation height is not only visible between neighboring rows of nickel atoms, but also between neighboring rows of oxygen atoms. We can interpret this contrast pattern in terms of a magnetic double tip (see [13] for a detailed discussion). If two magnetic atoms next to each other contribute significantly to the atomic scale contrast, one of them could interact magnetically with a nickel atom while the other one is already on top of an oxygen atom. The presence of a magnetic double tip is supported by two peculiar features visible in the line section along the [100]-direction, cf. Fig. 13.4b: (1)

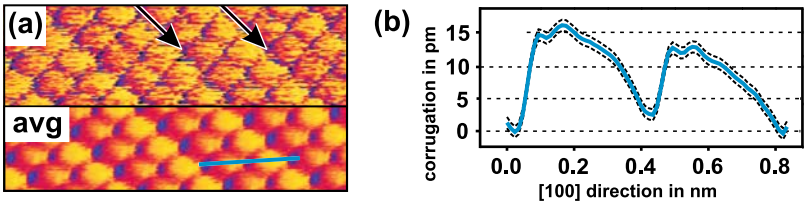

Fig. 13.4. (**a**) MExFM image (*top*) and the corresponding unit cell averaged image (*bottom*) obtained with a magnetic double tip on NiO(001). The *arrows* indicate the darker rows of Ni-atoms. (**b**) Line section along the [100] direction. The apparent magnetic contrast on neighboring oxygen rows and the asymmetric shape of the minima, which are also much narrower than the wide maxima, indicate the presence of a wedge-shaped blunt two atom tip apex. Parameters: $B = 5\,\mathrm{T}$, $f_0 = 159\,\mathrm{kHz}$, $c_z = 34.0\,\mathrm{N/m}$, $A_0 = \pm 6.3\,\mathrm{nm}$, $\Delta f = -20.5\,\mathrm{Hz}$

the maxima are wider than the minima and (2) the line shape is asymmetric. Feature (1) indicates a blunt tip and feature (2) a wedge-shaped tip. Subsuming (1) and (2) a tip apex consisting of two laterally and vertically displaced Fe atoms would explain the observed line shape. Note that none of these features are found in the symmetric line section of Fig. 13.3b, which indicates a single atom tip-apex. We can exclude a superexchange mechanism between the nickel atoms below the surface oxygen atoms and the iron tip as well as a direct magnetic exchange due to a small magnetic moment on the oxygen atoms, as it has been predicted in [24], because such a modulation must be always visible, but it is, e.g., not visible in Fig. 13.2c.

In Sect. 13.2 we already pointed out that even an external flux density of 5 T, which is much larger than the saturation magnetic polarization of the tip material, is not necessarily sufficient to fully align the magnetic moment of the foremost tip atom. This is shown in Fig. 13.5. Both images show the same area on NiO(001) with an atomic scale defect in the lower left corner, which can be used as a marker. Comparing (a) and (b) one can clearly detect a contrast reversal, i.e., darker rows of nickel atoms in (a) appear brighter in (b) and vice versa. Such a contrast reversal can be explained by a change of the orientation of the foremost tip atom. Since we neither observed a bump or a hole in the imaged area, we have no indication of a material transfer between tip and surface. In this context, it is important to remember that atomic structure and orientation of atomic magnetic moments are interrelated via spin–orbit coupling, which is the origin of the magneto-crystalline anisotropy energy. Hence, a reconfiguration in the tip apex region was most likely responsible for the reorientation of the magnetic moment of the foremost tip apex atom.

Note that the magnetic moments on NiO(001) are canted. Thus, if the magnetic moment at the tip-apex is canted as well, a contrast reversal does not require a flip of the magnetic moment of the foremost tip atom by 180° [13].

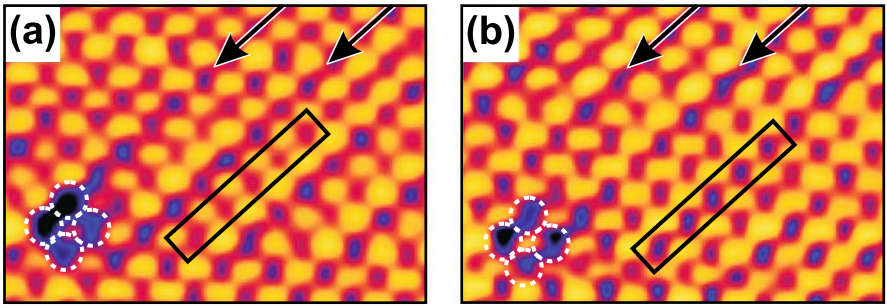

Fig. 13.5. Two low pass filtered MExFM images of NiO(001). After recording image (**a**) and before recording image (**b**) a tip reconfiguration occurred, which resulted in a reversal of the magnetic contrast, i.e., darker rows of nickel atoms appear brighter and vice versa with respect to the *encircled marker* defect in the *lower left corner* (see *arrows* and *rectangles* in the images). Parameters: $B = 5\,\mathrm{T}$, $f_0 = 159\,\mathrm{kHz}$, $c_z = 34.0\,\mathrm{N/m}$, $A_0 = \pm 6.3\,\mathrm{nm}$, $\Delta f = -21.0\,\mathrm{Hz}$

Furthermore, even a large external magnetic flux density does not exclude such a reorientation of the magnetic moment due to a reconfiguration, because the magnetic exchange energy between neighboring atoms at the tip apex can be much larger than the Zeeman energy of the external flux density.

13.4 Fe/W(001)

As a second specimen, we studied the iron monolayer (ML) on tungsten. Unlike the insulating NiO(001) sample Fe/W(001) is an itinerant metallic system. Surprisingly, an ML of Fe pseudomorphically grown on W(001) is not ferromagnetic. Due to strong hybridization with the substrate, it exhibits an antiferromagnetic c(2×2) order with out-of plane anisotropy, cf. Fig. 13.6a [25]. However, already two atomic layers show the prototypical ferromagnetism of this material. In the ML of Fe electrons are not as strongly correlated as in NiO. Hence, density functional calculations are less complex, which allows implementing realistic multi-atom tips and relaxation effects [14, 14a, 15]. Moreover, since an Fe coated tip is used here, only one relevant chemical species is present in this tip–sample system leading to an experimentally easier situation than for NiO(001). As an itinerant two-dimensional antiferromagnetic metal with delocalized *d*-electrons, the Fe ML is magnetically quite different from the insulating NiO, where the *d*-electrons are strongly localized and coupled via superexchange. Therefore, it is very interesting to compare the experimental findings for both systems with each other.

To prepare a suitable sample it is mandatory to start with a clean W(001) substrate. This is achieved by flashing the substrate at 2,100°C for 10 s and by annealing at 1,300°C in oxygen ($\approx 10^{-6}$ mbar). After such a treatment of the substrate, we deposited slightly more than one atomic layer of Fe at

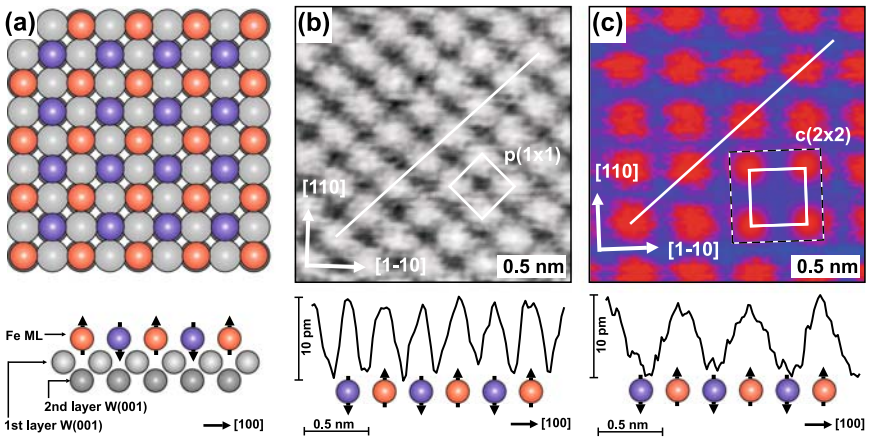

Fig. 13.6. (**a**) Structure of the Fe/W(001) sample. The ML of Fe grows pseudomorphically on W(001) as shown in the side view and exhibits a checkerboard antiferromagnetic order. (**b**) NC-AFM image of the Fe ML obtained with a magnetically insensitive tip. The contrast pattern reflects the p(1 × 1) chemical unit cell, i.e., every Fe atom is represented by a protrusion, (**c**) MExFM image of the Fe ML. The c(2 × 2) arrangement of protrusions with respect to the underlying tungsten substrate reflects the magnetic surface unit cell obtained with a magnetically sensitive tip. The enframed inset displays the result of a simulation employing density functional theory (DFT) based on first principles calculations, which is in very good agreement with the experimental data [14–16]. Note that the magnetic signal of 10 pm is much larger than on NiO(001), cf. line section. Parameters: (**b**) $B = 5\,\mathrm{T}$, $f_0 = 156\,\mathrm{kHz}$, $c_z = 32.5\,\mathrm{N/m}$, $A_0 = \pm 5.0\,\mathrm{nm}$, $\Delta f = -28.5\,\mathrm{Hz}$; (**c**) same except $\Delta f = -14.8\,\mathrm{Hz}$

an elevated temperature of about 600 K onto the substrate. As a result, the substrate is completely covered by a pseudomorphically grown wetting layer, i.e., the antiferromagnetic ML with out-of-plane anisotropy. Excess iron forms ferromagnetic second layer islands with fourfold in-plane anisotropy [26] and stripes along substrate steps (step flow growth).

Atomically resolved data on the Fe ML revealed two different contrast patterns. In Fig. 13.6b protrusions are arranged in a p(1 × 1) array with respect to the W(001) substrate. Thus, every Fe atom is imaged as protrusion as expected for a purely chemical contrast of a pseudomorphically grown ML. On the other hand, protrusions in Fig. 13.6c are arranged in a c(2 × 2) array with respect to the W(001) substrate, i.e., only every second Fe atom is imaged as protrusion. This contrast pattern reflects the symmetry of the antiferromagnetic surface unit cell. Both images were actually recorded with the same iron coated tip, but in between tip changes occurred. These tip changes resulted in a magnetically sensitive, cf. Fig. 13.6b, and a magnetically insensitive, cf. Fig. 13.6c, tip configuration. Possible mechanisms for such tip changes are explained in Sect. 13.2.

One important and very encouraging result on the Fe ML is the large magnetic corrugation amplitude of 10 pm, cf. line section of Fig. 13.6c. It is in fact as large as the chemical corrugation amplitude, cf. line section of Fig. 13.6b. Compared to the magnetic corrugation amplitude of 1.5 pm on NiO(001), such a large signal is readily detectable and promising with respect to future investigations using MExFM (see Sect. 13.5). The origin of the larger signal is the farther extension of the spin-carrying *d*-electrons into the vacuum region of the Fe ML compared to the localized *d*-electrons in nickel oxide. Another possible reason is the out-of-plane orientation of the magnetic moments of the Fe ML. If the tip magnetic moments are oriented parallel to the external magnetic flux density, i.e., perpendicular to the surface, the resulting magnetic signal is larger than for canted magnetic moments as on NiO(001).

Comparing the line sections of MExFM data on NiO(001), cf. Fig. 13.2c, and the Fe ML on W(001), cf. Fig. 13.6c, reveals a surprising difference. On NiO(001) the magnetic exchange interaction is added on top of the chemical interaction, i.e., oxygen atoms are imaged as protrusions and nickel atoms are imaged as depressions, but with a height modulation on neighboring rows of nickel atoms, which reflects the row-wise antiferromagnetic order. On the other hand, only every second iron atom of the ML is imaged as protrusion. This is surprising, because magnetic exchange and chemical interaction are both electron mediated and of short range. Therefore, each iron atom should appear as protrusion due to the chemical interaction and the additional magnetic exchange interaction should result in a height modulation, which reflects the checkerboard type antiferromagnetic order.

The origin of this peculiar contrast pattern is revealed by theoretical studies, which are presented in more detail in Chap. 14 of this book [16]. By employing a multiatom iron tip with magnetic moment pointing toward the surface, distance dependent force curves could be calculated on the three high symmetry points, i.e., on top of iron atoms with parallel and antiparallel magnetic moments, respectively, and in between at the hollow sites. In an intermediate distance regime these curves exhibit a cross over, where the total short-range electron mediated force, i.e., chemical plus magnetic exchange force, on the parallel and hollow site is equal. Therefore, only the iron atoms with antiparallel aligned magnetic moments appear as protrusions. Using these force data and long-range van der Waals forces stemming from a tip with 8 nm radius the experimentally observed contrast pattern could be reproduced, cf. enframed inset in Fig. 13.6c. Thus, we can conclude that the missing maxima on every second iron atom are due to a competition between magnetic exchange and chemical interaction, but not because of an absence of the latter [14].

13.5 Future Perspectives

What can be expected in future from MExFM? One can think of many interesting experiments, e.g., investigating the structure of domain walls or more complex magnetic structures like spin spirals in electrically insulating systems with atomic resolution. Note that recently such spin spirals have been observed on metallic surfaces by SP-STM and attracted a lot of attention [27]. Magnetic sensitive force spectroscopy allows to study the distance dependence of the various types of magnetic exchange forces (e.g., superexchange, double exchange, RKKY, etc.), which can be directly compared with theory. Moreover, apart from MExFM only SP-STM can obtain a magnetic contrast with atomic resolution, but the latter can only be applied to electrically conductive surfaces. Such a limitation does not exist for a force based technique, which is particularly useful, if magnetic properties of single atoms or molecules on surfaces should be investigated. On metallic substrates strong hybridization occurs, which can be avoided if insulating substrates are utilized instead. Even on conductive samples MExFM is very useful, because it is sensitive to a different quantity, i.e., forces instead of the local density of states (LDOS). Hence, complementary information can be extracted.

We would like to thank U.H. Pi and acknowledge financial support from the Deutsche Forschungsgemeinschaft (SFB 668-A5 and Graduiertenkolleg 611).

References

1. G. Binnig, H. Rohrer, Helv. Phys. Acta. **55**, 726 (1982)
2. G. Binnig, C.F. Quate, C. Gerber, Phys. Rev. Lett. **56**, 930 (1986)
3. Y. Martin, H.K. Wickramasinghe, Appl. Phys. Lett. **50**, 1455 (1987)
4. U. Hartmann, Annu. Rev. Mater. Res. **29**, 53 (1999)
5. A. Schwarz, R. Wiesendanger, Nano Today **3**, 28 (2008)
6. R. Wiesendanger, G. Güntherodt, H.J. Güntherodt, R.J. Gambino, R. Ruf, Phys. Rev. Lett. **65**, 247 (1990)
7. M. Bode, Rep. Prog. Phys. **66**, 523 (2003)
8. R. Wiesendanger, D. Bürgler, G. Tarrach, A. Wadas, D. Brodbeck, H.J. Güntherodt, G. Güntherodt, R.J. Gambino, R. Ruf, J. Vac. Sci. Technol. B **9**, 519 (1990)
9. U. Kaiser, A. Schwarz, R. Wiesendanger, Nature **446**, 522 (2007)
10. H. Hosoi, K. Sueoka, K. Hayakawa, K. Mukasa, in *Noncontact Atomic Force Microscopy*, ed. by S. Morita, R. Wiesendanger, E. Meyer (Springer, Berlin, 2002), p. 126; Hosoi, K. Sueoka, K. Mukasa, Nanotechnology **15**, 505 (2004)
11. F.J. Giessibl, in *Noncontact Atomic Force Microscopy*, ed. by S. Morita, R. Wiesendanger, E. Meyer (Springer, Berlin, 2002), p. 11
12. M. Liebmann, A. Schwarz, S.M. Langkat, R. Wiesendanger, Rev. Sci. Instrum. **73**, 3508 (2002)
13. U. Kaiser, A. Schwarz, R. Wiesendanger, Phys. Rev. B **77**, 104418 (2008)
14. R. Schmidt, C. Lazo, H. Hölscher, U.H. Pi, V. Caciuc, A. Schwarz, R. Wiesendanger, and S. Heinze, Nano Lett., **9**, 200 (2009)

15. C. Lazo, V. Caciuc, H. Hlscher, and S. Heinze, Phys. Rev. B **78**, 214416 (2008)
16. C. Lazo, V. Caciuc, H. Hlscher, and S. Heinze, in *First Principles Simulation of Magnetic Exchange Force Microscopy on Fe/W(001)*, ed. by S. Morita, F.-J. Giessibl, R. Wiesendanger (Springer-Verlag Berlin-Heidelberg, 2009) pp. 287–302
17. T. Okazawa, Y. Yagi, Y. Kido, Phys. Rev. B **67**, 195406 (2003)
18. F.U. Hillebrecht, H. Ohldag, N.B. Weber, C. Bethke, U. Mick, M. Weiss, J. Bahrdt, Phys. Rev. Lett. **86**, 3419 (2001)
19. H. Hosoi, K. Sueoka, K. Hayakawa, K. Mukasa, Appl. Surf. Sci. **157**, 218 (2000)
20. W. Allers, S. Langkat, R. Wiesendanger, Appl. Phys. A **72**, S27 (2001)
21. R. Hoffmann, M.A. Lantz, H.J. Hug, P.J.A. van Schendel, P. Kappenberger, S. Martin, A. Baratoff, H.J. Güntherodt, Phys. Rev. B **67**, 085402 (2003)
22. M.R. Castell, S.L. Dudarev, G.A.D. Briggs, A.P. Sutton, Phys. Rev. B **59**, 7342 (1999)
23. S. Ciraci, A. Baratoff, I.P. Batra, Phys. Rev. B **41**, 2763 (1990)
24. H. Momida, T. Oguchi, Surf. Sci. **590**, 42 (2005)
25. A. Kubetzka, P. Ferriani, M. Bode, S. Heinze, G. Bihlmayer, K. von Bergmann, O. Pietzsch, S. Blügel, R. Wiesendanger, Phys. Rev. Lett. **94**, 087204 (2005)
26. K. von Bergmann, M. Bode, R. Wiesendanger, Phys. Rev. B **70**, 174455 (2004)
27. M. Bode, M. Heide, K. von Bergmann, P. Ferriani, S. Heinze, G. Bihlmayer, A. Kubetzka, O. Pietzsch, S. Blgel, R. Wiesendanger, Nature **447**, 190 (2007)